AEROELASTIC STABILITY OF COMPOSITE BEARINGLESS ROTOR BLADES

Xu Ming
Aircraft Division, Naval Research Center
Shanghai, P.R. China
Wang Shi-cun
Nanjing Aeronautical Institute
Nanjing, P.R. China

Abstract

The present analysis makes the first attempt to establish and define the generalized constitutive equations for composite laminated beams with large bending–torsion coupled deflection, in which the constitutive equations of the relevant problem for laminated plates or shells are included formally. The effects of geometrical parameters of the flexure on aeroelastic stability of isotropic bearingless blades are studied first. For composite blades, the transverse shear stress is considered in the constitutive equation and analytical formulae. Then the flutter stability of flap bending, lead–lag bending, and torsion of composite rotor blades in hover is investigated by using a finite element formulation based on Hamilton's principle. The emphasis is put on analyzing the influences of layered angles and stacking sequence on dynamic stabilities of composite hingeless and bearingless rotor blades. Moreover the importances of some new coupling stiffness coefficients, such as EAe_b and EB_{21},are discussed for certain configuration.

Introduction

In recent years, there has been considerable interest in bearingless rotor designs with an eye toward mechanical simplicity and increased maintainability. The bearingless blade has an elastic flexure consisting of flexbeams and a torque tube to facililate pitch changes. An example that has been tested in flight and wind tunel is the Boeing Vertol designed Bearingless Main Rotor [1]. Generally, the articulated and hingeless blades are refered to as single–load–path blades and the bearingless blade as a multiple–load–path blade. This is because the blade loads can be transmitted to the hub by redundant paths of the flexure in the case of a bearingless blade. Recently, there have been some attempts to analyze bearingless blades, the most notable working is that of Sivaneri and Chopra [2]. But they did not seem to investigate systematically the effects of flexure's geometrical dimensions on dynamic stability of the bearingless blade.

Another important recent development is that composite materials have been used widely in the construction of rotor blades. Composites have better fatigue characteristics than metals, a factor which is very significant to rotors. Advanced composites also hold the promise of lower production costs and lower dynamic stresses and vibrations accomplished through efficient, optimized structures. In 1979, Mansfield and Sobey [3] made a pioneering attempt to develop the stiffness properties of graphite fiber composite rotor blades and they also tried to explore the potential of this model for aeroelastic tailoring. A comprehensive and important study by Hong and Chopra [4],[5] presented, for the first time, an aeroelsastic model for a composite rotor blade. However, there is no transverse shear stress in the researches mentioned above, probably due to the characteristics of analyzed configurations of composite rotor blades. In addition, the influence of multiple load paths of composite bearingless rotor blades on aeroelastic stability has not yet fully understood, though Hong and Chopra gave some results about the aeroelastic stability of a composite bearingless rotor in Ref.5.

In present paper, the effects of geometrical parameters of the flexure on aeroelastic stability of isotropic bearingless blades are first studied systematically. For composite blades, the transverse shear stress is considered in the constitutive equation and analytical formulae. Then, the flutter stability of flap bending, lead–lag bending, and torsion of composite rotor blades in hover is investigated by using a finite element formulation based on Hamilton's principle. The present emphasis is put on analyzing the influences of layered orientations and stacking sequences on dynamic stabilities of composite hingeless and bearingless rotor blades. Moreover the importances of some new terms or parameters are also discussed for unsymmetric configurations.

Strain Energy Of A Composite Blade

The rotor blade is treated as an elastic beam rotating with constant angular velocity Ω. The blade spar is represented by a laminated beam (Fig.1). It is assumed that the beam provides the required blade structural stiffness. The rectangular coordinate system, x, y, z is attached to the undeformed blade, the x–axis coincides with the elastic axis, and the y–axis is in the plane

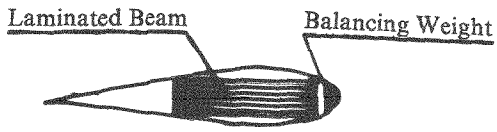

Fig.1 Composite blade section

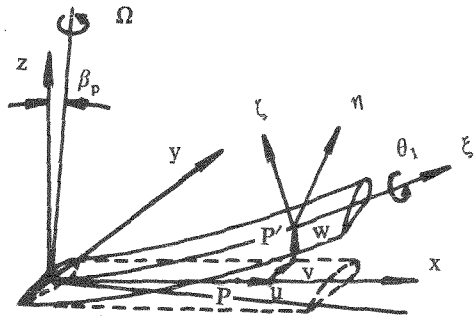

Fig.2 Blade coordinate system and deflection

of rotation (Fig.2). The blade is preconed through a small angle β_p. A point P on the undeformed elastic axis undegoes displacements u,v,w in the x,y,z directions respectirely, and occupies the position P′ on the deformed elastic axis. Then the blade cross–section containing P′ undegoes a rotation $\theta_1$about the deformed elastic axis. The angle $\theta_1$which represents the blade total geometric pitch including pretwist is given in Ref.2. The orthogonal coordinate system ξ,η,ζ is attached to the deformed blade such that the ξ axis is tangential to the deflected elastic axis and the η and ζ axes are the principal axes of the cross section.

The stress–strain relation for the kth lamina of the laminated beam is given in Ref.6 as follows

$$\begin{Bmatrix}\sigma_{xx}\\ \tau_{x\eta}\\ \tau_{x\zeta}\end{Bmatrix}^{(k)}=\begin{bmatrix}Q_{11} & Q_{16} & 0\\ Q_{16} & Q_{66} & 0\\ 0 & 0 & Q_{55}\end{bmatrix}^{(k)}\begin{Bmatrix}\varepsilon_{xx}\\ r_{x\eta}\\ r_{x\zeta}\end{Bmatrix} \quad (1)$$

The equations of motion are obtained using Hamilton's principle,

$$\triangle=\int_{t_1}^{t_2}(\delta U-\delta T-\delta W)dt=0 \quad (2)$$

where δU,δT, and δW are, respectively, the variation of strain energy, the variation of kinetic energy, and the virtual work done. The variation of strain energy for the composite blade is expressed

$$\delta U=\int_0^l\iint_A\begin{bmatrix}\sigma_{xx}^{(k)} & \tau_{x\eta}^{(k)} & \tau_{x\zeta}^{(k)}\end{bmatrix}\begin{Bmatrix}\delta\varepsilon_{xx}\\ \delta r_{x\eta}\\ \delta r_{x\zeta}\end{Bmatrix}dA\,dx$$

$$\int_0^l\iint_A[\varepsilon_{xx}\ r_{x\eta}\ r_{x\zeta}]\begin{bmatrix}Q_{11} & Q_{16} & 0\\ Q_{16} & Q_{66} & 0\\ 0 & 0 & Q_{55}\end{bmatrix}^{(k)}\delta\begin{Bmatrix}\varepsilon_{xx}\\ r_{x\eta}\\ r_{x\zeta}\end{Bmatrix}dA\,dx \quad (3)$$

Where
$$\varepsilon_{xx}=u'+v'^2/2+w'^2/2-\lambda\phi''+(\eta^2+\zeta^2)(\theta'\hat{\phi}'+\hat{\phi}'^2/2)-v''(\eta cos\theta_1-\zeta sin\theta_1)-w''(\eta sin\theta_1+\zeta cos\theta_1)$$
$$r_{x\eta}=-\hat{\zeta}\phi'$$
$$r_{x\zeta}=\hat{\eta}\phi'$$
$$\hat{\zeta}=\zeta+\partial\lambda/\partial\eta,\ \hat{\eta}=\eta-\partial\lambda/\partial\zeta$$

and λ is the warping function.

The strain–displacement relations for moderate deflections are take from Hodges and Dowell's [7], where nonlinear terms up to second order are retained. The strain energy expression δU can be derived and written in nondimensional form

$$\delta U/(m_o\Omega^2R^3)=$$
$$\int_o^l\{EA(u'+v'^2/2+w'^2/2)\delta u'$$
$$+EA[k_A^2\theta'\hat{\phi}-e_a(v''cos\theta_1+w''sin\theta_1)]\delta u'+[EAe_b(v''sin\theta_1-w''cos\theta_1)+k_{p3}(\hat{\phi}'+v''w')\ ]\delta u'$$
$$+F(v'\delta v'+w'\delta w')+GJ(\hat{\phi}'\delta\hat{\phi}'+\hat{\phi}'w'\delta v''+\hat{\phi}'v''\delta w'+v''w'\delta\hat{\phi}')+[Fk_A^2(\theta'+\hat{\phi}')-EAk_A^4\theta'^2\hat{\phi}'+EAk_A^2e_a\theta'(v''cos\theta_1+w''sin\theta_1)-EAk_A^2e_b\theta'(v''sin\theta_1-w''cos\theta_1)-k_{p3}\hat{\phi}'k_A^2\theta'+EB_1\theta'^2\hat{\phi}'$$
$$-EB_2\theta'(v''cos\theta_1+w''sin\theta_1)+EB_{21}\theta'(v''sin\theta_1-w''cos\theta_1)+k_{p4}\theta'\hat{\phi}']\delta\hat{\phi}'$$
$$+[-k_{p2}(v''sin\theta_1-w''cos\theta_1)+k_{p6}(v''cos\theta_1+w''sin\theta_1)+k_{p4}\theta'\hat{\phi}'+k_{p5}\hat{\phi}''+k_{p3}(u'+v'^2/2+w'^2/2)]\delta\hat{\phi}'$$
$$+[EC_1\phi''-EC_2(v''sin\theta_1-w''cos\theta_1)+k_{p5}\hat{\phi}']\delta\hat{\phi}''$$
$$+[-Fe_acos\theta_1+k_{p3}e_a\hat{\phi}'cos\theta_1+Fe_bsin\theta_1-k_{p3}e_b\hat{\phi}'sin\theta_1+(EI_zcos^2\theta_1+EI_ysin^2\theta_1)v''+(EI_z-EI_y)sin2\theta_1w''/2-EAe_a^2(v''cos^2\theta_1+w''sin2\theta_1/2)+EAe_be_a(v''sin2\theta_1-w''cos2\theta_1)-EAe^2{}_b(v''sin^2\theta_1-w''sin2\theta_1/2)+(EAe_ak_A^2-EB_2)$$

$$
\begin{aligned}
&\theta'\hat{\Phi}'cos\theta_1 - (EAe_b k_A^2 - EB_{21})\theta'\hat{\Phi}'sin\theta_1 \\
&- EC_2 sin\theta_1 \hat{\Phi}'' - k_{p2} sin\theta_1 \hat{\Phi}' \\
&\quad + k_{p6}\hat{\Phi}'cos\theta_1]\delta v'' \\
&+ [-Fe_a sin\theta_1 + k_{p3} e_a \hat{\Phi}' sin\theta_1 - Fe_b cos\theta_1 \\
&+ k_{p3} e_b \hat{\Phi}' cos\theta_1 \\
&\quad + \left(EI_z sin^2\theta_1 + EI_y cos^2\theta_1 \right) w'' \\
&+ (EI_z - EI_y) sin2\theta_1 v''/2 \\
&\quad - EAe_a^2 (v'' sin2\theta_1/2 \\
&+ w'' sin^2\theta_1) \\
&\quad + EAe_a e_b (-v'' cos2\theta_1 - w'' sin2\theta_1) \\
&+ EAe^2{}_b (v'' sin2\theta_1/2 - w'' cos^2\theta_1) \\
&\quad + (EAe_a k_A^2 \\
&- EB_2)\theta'\hat{\Phi}' sin\theta_1 + (EAe_b k_A^2 - EB_{21})\theta'\hat{\Phi}' \\
&\cdot cos\theta_1 + EC_2 \hat{\Phi}'' cos\theta_1 + k_{p2}\hat{\Phi}' cos\theta_1 \\
&+ k_{p6}\hat{\Phi}' sin\theta_1]\delta w'' \\
&\quad + [Fe_a (v'' sin\theta_1 - w'' cos\theta_1) \\
&- k_{p3} e_a \hat{\Phi}' (v'' sin\theta_1 - w'' cos\theta_1) \\
&\quad + Fe_b (v'' cos\theta_1 \\
&+ w'' sin\theta_1) - k_{p3} e_b \hat{\Phi}' (v'' cos\theta_1 + w'' sin\theta_1) \\
&+ (EI_z - EI_y) < (w''^2 - v''^2) sin2\theta_1/2 \\
&+ v'' w'' cos2\theta_1 > \\
&\quad - (k_{p2} sin\theta_1 - k_{p6} cos\theta_1)\hat{\Phi}' w'' \\
&- (k_{p2} cos\theta_1 + k_{p6} sin\theta_1)\hat{\Phi}' v'']\delta\hat{\Phi} \\
&+ [k_{p3} u' - k_{p2} (v'' sin\theta_1 - w'' cos\theta_1) \\
&+ k_{p6} (v'' cos\theta_1 + w'' sin\theta_1)](w'\delta v'' + v''\delta w') \\
&+ (-k_{p2} sin\theta_1 + k_{p6} cos\theta_1) v'' w' \delta v'' \\
&+ (k_{p2} cos\theta_1 + k_{p6} sin\theta_1) v'' w' \delta w''\} \; dx \qquad (4)
\end{aligned}
$$

where m_0 is the reference mass per unit length, and R is the rotor radius.

The centrifugal force F(x) in Eq.(4) is obtained as

$$
\begin{aligned}
F(X) = EA\{&u' + v'^2/2 + w'^2/2 + k_A^2 \theta'\hat{\Phi} \\
&- e_a (v'' cos\theta_1 \\
&\quad + w'' sin\theta_1) \\
&+ e_b (v'' sin\theta_1 - w'' cos\theta_1)\} + K_{p3}\hat{\Phi}' \qquad (5)
\end{aligned}
$$

The effective section stiffnesses and the coupling stiffness coefficients are

$$
\left.
\begin{aligned}
EA &= \sum_{k=1}^{N} \iint Q_{11}^{(k)} d\eta d\zeta \\
EI_y &= \sum_{k=1}^{N} \iint Q_{11}^{(k)} \zeta^2 d\eta d\zeta \\
EI_z &= \sum_{k=1}^{N} \iint Q_{11}^{(k)} \eta^2 d\eta d\zeta \\
EAk_A^2 &= \sum_{k=1}^{N} \iint Q_{11}^{(k)} (\eta^2 + \zeta^2) d\eta d\zeta \\
GJ &= \sum_{k=1}^{N} \iint \left(Q_{55}^{(k)} \hat{\eta}^2 + Q_{66}^{(k)} \hat{\zeta}^2 \right) d\eta d\zeta \\
EAe_a &= \sum_{k=1}^{N} \iint Q_{11}^{(k)} \eta d\eta d\zeta \\
EAe_b &= \sum_{k=1}^{N} \iint Q_{11}^{(k)} \zeta d\eta d\zeta \\
EB_1 &= \sum_{k=1}^{N} \iint Q_{11}^{(k)} (\eta^2 + \zeta^2)^2 d\eta d\zeta \\
EB_2 &= \sum_{k=1}^{N} \iint Q_{11}^{(k)} \eta (\eta^2 + \zeta^2) d\eta d\zeta \\
EB_{21} &= \sum_{k=1}^{N} \iint Q_{11}^{(k)} \zeta (\eta^2 + \zeta^2) d\eta d\zeta \\
EC_1 &= \sum_{k=1}^{N} \iint Q_{11}^{(k)} \lambda^2 d\eta d\zeta \\
EC_2 &= \sum_{k=1}^{N} \iint Q_{11}^{(k)} \zeta\lambda d\eta d\zeta
\end{aligned}
\right\} \qquad (6)
$$

$$
\left.
\begin{aligned}
k_{p2} &= \sum_{k=1}^{N} \iint Q_{16}^{(k)} \hat{\zeta}\zeta d\eta d\zeta \\
k_{p3} &= \sum_{k=1}^{N} \iint Q_{16}^{(k)} \hat{\zeta} d\eta d\zeta \\
k_{p4} &= -\sum_{k=1}^{N} \iint Q_{16}^{(k)} \hat{\zeta} (\eta^2 + \zeta^2) d\eta d\zeta \\
k_{p5} &= -\sum_{k=1}^{N} \iint Q_{16}^{(k)} \hat{\zeta}\lambda d\eta d\zeta \\
k_{p6} &= -\sum_{k=1}^{N} \iint Q_{16}^{(k)} \hat{\zeta}\eta d\eta d\zeta
\end{aligned}
\right\} \qquad (7)
$$

Obviously, all the coupling stiffness coefficients in Eq.(7) are related to the properties of composite materials, so they will become zero for isotropic blades.

Two new constants EAe_b and EB_{21} (see Eq.(6)), neglected in Ref.4 and 5, are included in the present expression of energy. For an isotropic beam, the two coefficients will vanish because the coordinates η, ζ coincide with the geometrically symmetrical axes of the beam's cross section. For an anisotropic laminate, however, the geometrical symmetry can not be regarded as the physical symmetry of the cross section. Consequently, $EAe_b$and EB_{21}may not be zero in this case. On the other hand, $EAe_b$is in the same order of magnitude as k_{p3}. Therefore, these terms associated with $EAe_b$and EB_{21}, especially EAe_b, should be included in the dynamic formulation of composite blades.

The variation of kinetic energy δT is the same for a composite blade as for an isotropic blade, and given in nondimensional form in Ref.7. The aerodynamic force are obtained using the quasisteady strip theory approximation. Forces of noncirculatory origin are also included. The induced inflow is assumed uniform and steady. The details of the aerodynamic forces in the expression for δW are taken from Ref.2.

Finite Element Discretization

A approximate treatment is made for the finite element discretization of a composite blade. The rotating angles of the cross section of the blade are assumed to equal the slopes of the beam's axes. This assumption is resonable and suitable for the dynamic stability of helicopter rotor blades with large aspect ration, so that the finite element discretization of a composite blade becomes completely similar to that of an isotropic blade.

The blade and flexbeams are divided into a number of beam elements. Each element consists of two end nodes and three internal nodes, which result in a total of fifteen degrees of freedom [2]. Each of the end nodes has six degrees of freedom, namely u,v,v',w,w', and $\hat{\phi}$. Among the three internal nodes, two are for u and one for $\hat{\phi}$. The distribution of the deflection over an element is represented in terms of element degrees of freedom and shape functions.

Hamilton's principle (Eq.(2)) is discretized as

$$\sum_{i=1}^{N} (\delta U_i - \delta T_i - \delta W_i) = 0 \qquad (8)$$

where δU_i, $\delta T_i$and $\delta W_i$are the virtual strain energy, the virtual kinetic energy and the virtual work contribution of the ith–element.

The assembly of N elements yields the equations of motion in terms of nodal displacements, expressed as

$$[M(q)]\{\ddot{q}\} + [C(q)]\{\dot{q}\} + [K(q)]\{q\} = \{Q\} \qquad (9)$$

where [M],[C] and [K] are respectively the global inertia, damping and stiffness matrices. These equations are nonlinear in {q}.

In the present analysis, two typical configurations are selected to study the aeroelastic stability of composite blades. One model is for a composite hingeless blade, another for a composite bearingless rotor blade with the flexure consisting of two parallel laminated beams (see Figure 3). Here, the torque tube in the flexure is assumed to be extremely stiff in torsion and very soft in flexure, so that there is no need to depict the torque tube in the analytical model (Fig.3b). For composite bearingless blades, the flexure–beam offsets $\eta_1$and $\eta_2$from the axis of the blade are equal to b / 4 and –b / 4 respectively.

Special displacement compatibility conditions at the clevis , which connectes the blade with the flexure, are also the same as that in Ref.2.

Solution procedures

The first step is to obtain the steady trim solution. The blade steady deflected position is calculated from the nonlinear Eq.(9), after dropping time dependent terms. Through an iterative procedure, the solution can be calculated numerically. There are two major differences between the trim solution procedure for the hingeless blade and that for the bearingless blade:

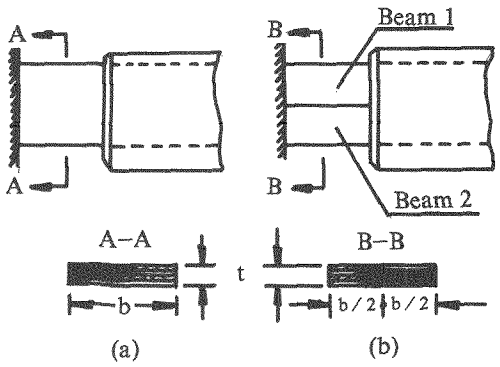

Fig.3 Analytical models of composite hingeless and bearingless blades

1. The centrifugal force distribution F(x) is known a priori only over the outboard blade, and unknown over the flexure because of the multiple load paths involved. In obtaining the linear estimation of the steady equations, it is assumed that the centrifugal force in each of the inboard beam is in the ratio of its tensile stiffness EA. Then, at succesive iterations the centrifugal force distribution is updated using Eq.(5).

2. The pitch distribution is known previously for the outboard blade, and unknown for the flexbeams. The pitch distribution along the flexbeams is assumed to be linear for the first iteration. This distribution is updated at successive iterations based on the torsional deflection.

The second step is to obtain the coupled rotating normal modes of vibration about the equilibrium position. For this the damping matrix and aerodynamic terms are removed from Eq.(9), and the equations are linearized assuming the motion be small perturbation about the steady position. The resulting equations are solved as an algebraic eigenvalue problem.

The last step is to calculate the flutter stability. Using several natural vibration modes, the stability equations are transformed to the modal space and the resulting normal mode equations are solved as complex eigenvalue problems. The aeroelastic stability of composite rotor blades can be analyzed through the root locus plots for eigenvalues.

Results and Discussion

Numerical results are presented for four different rotor configurations–isotropic hingeless and bearingless rotors, as well as composite hingeless and bearingless rotors. The chordwise offsets of the center of mass, the aerodynamic center, and torsion center from the elastic axis are considered to be zero. The section constants EB_1, EB_2, and the warping constants EC_1, EC_2, are taken to be zero. A precone (β_p) of 0.05

rad, lock number (r) of 5, and solidity ratio (σ) of 0.1 are used.

Isotropic Hingeless Rotor Blade

The blade properties selected for the dynamic analysis of the isotropic hingeless blade are taken from Ref. 8. Figure 4 shows the steady tip deflections for different levels of thrust C_T/σ (or θ). The fundamental torsional frequency is 5.0 for these results. The results of Hodges and Ormiston[8] are also shown in this figure. In Ref. 8, the steady deflections are obtained using the modal method with five nonrotating beam modes for each one of the deflections v_o, w_o, and $\hat{\Phi}_o$. The agreement between the two results is good except at high thrust levels where some deviation appears.

Isotropic Bearingless Rotor Blade

The outboard blade and the flexbeams are considered to be uniform. The offset of the elastic axis of the flexbeams from that of the outboard blade ($\eta_1 = -\eta_2$) is taken to be 0.4c, where c is the chord of the outboard blade. The length of the flexure is 0.25R. The blade properties are from Ref.2.

To examine the present formulation for multiple–load–path blades, a simple analytical model is considered, in which the pitch of the flexure is fixed at zero while the pitch of the outboard is varied. Figure 5 shows the root locus plot of the fundamental lead–lag modes as C_T/σ is varied from o to 0.2. It is seen that the lead–lag mode is unstable for C_T/σ higher than about 0.06. In this figure, the results from Ref.2 are also shown. The two results coincide with each other broadly.

Next, the influence of the geometrical parameters of the flexure on aeroelastic stability of an isotropic bearingless blade is studied. Figures 6 and 7 are the root locus plots of the fundamental lead–lag and flap modes with beam 2 moving forward (beam 1 fixed) or beam 1 moving backward (beam 2 fixed). Figure 6 indicates that with beam 2 moving forward (beam 1 fixed), the multiple–load–path system trends toward the stable area first, and then rapidly toward the unstable area for $\eta_2 > -c/4$. In figure 7, the stability

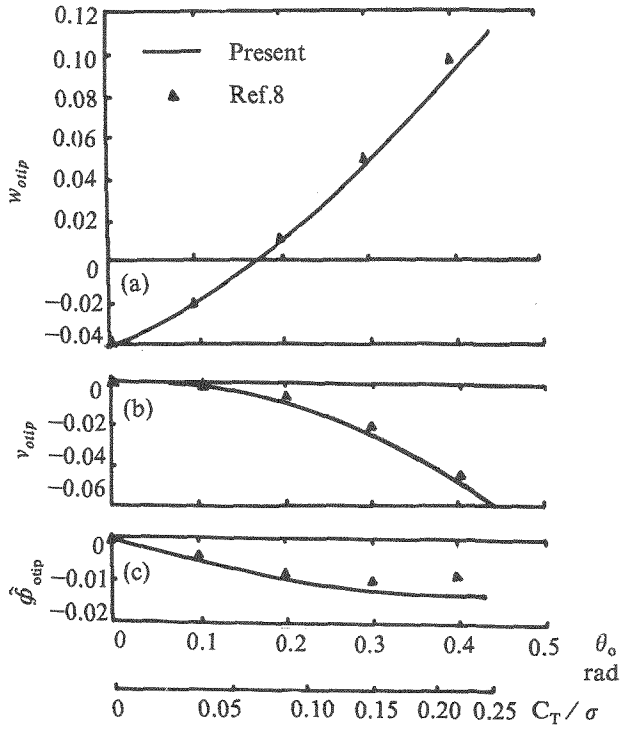

Fig.4 Steady tip deflections of an isotropic hingeless blade

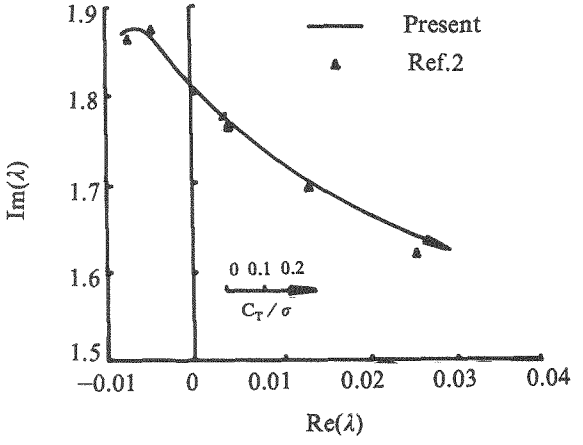

Fig.5 Root locus plot of lead–lag mode of isotropic bearingless blade (Zero inboard pitch)

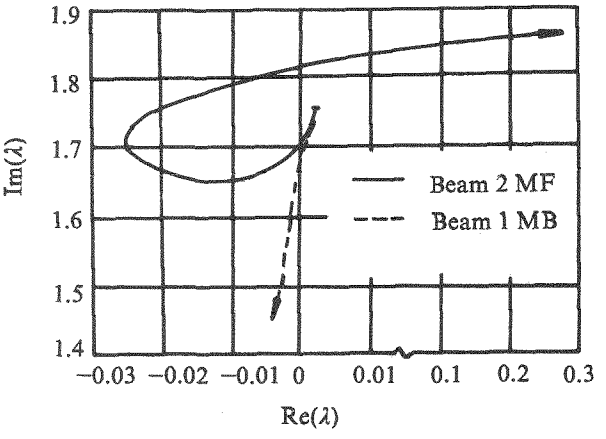

Fig.6 Effect of each–beam translation along y axis on lag–mode stability (MF / MB—one beam moved forward / backward while other fixed)

of flap mode is gradually reduced when beam 2 moves forward with beam 1 fixed. However, the backward movement of beam 1 (beam 2 fixed) only slightly changes the stability of the isotropic bearingless blade (see Fig.6 and Fig.7).

In analyzing the influence of two–beam distance

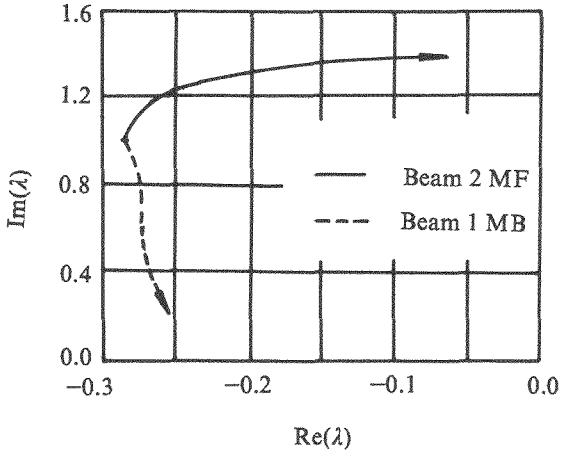

Fig.7 Effect of each –beam translation along y axis on flap–mode stability

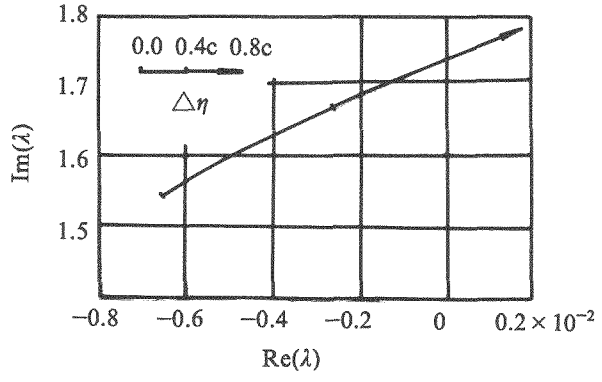

Fig.8 Effect of the distance between two beams on stability of lead–lag mode

on the dynamic stability of the bearingless blade, it is assumed that the geometrical center line (shear axis) of the flexure remains coincident with the elastic axis of blade, while the positions of beam 1 and beam 2 may vary with each other simultaneously. Figure 8 shows that the greater the distance between the two flexbeams, the less the stability of lead–lagmode. And the multiple–load–path system is stable until the distance ($\triangle\eta=\eta_1-\eta_2$) is around 0.65c.

Composite hingeless Rotor Blade

The structural configuration of a composite hingeless rotor blade is shown in Fig.3(a). The original data are the same as those used in the analysis of isotropic bearingless blades except for:

I. Material constants

$E_L=30\times10^6$psi $\quad r_{LT}=0.3$
$E_T=3\times10^6$psi $\quad r_{TL}=0.03$
$G_{LT}=1.2\times10^6$psi $\quad r_{TT}=0.5$
$G_{TT}=0.72\times10^6$psi

II. Airfoil characteristics

$c_l=5.7\alpha,\ c_d=0.01,\ c_{mac}=0.0,\ C_T/\sigma=0.1$

The fundamental lead–lag, flap, and torsion frequencies for a baseline configuration with zero ply angle are 1.52, 1.14, and 5.09 respeectively. For this, the laminate consists of graphite laminae with fibers parallel to the blade length. Stability results are calculated for three selected configurations (unsymmetric, symmetric, and antisymmetric configurations).

Figure 9 shows the root locus plots of the complex eigenvalues for lead–lag mode as a function of ply angle for the unsymmetric configuration. In this configuration, the laminae in the top half thickness have zero ply angles, and the laminae in the bottom half thickness are all oriented at the same ply angles. Seen from Fig.9, the system with positive ply angles becomes more stable than that with negative ply angles. And the maximum deviation between the two curves in Fig. 9 can be up to 15% around. It is clear enough to recognize the effect of the coupling coefficient EAe_b, always neglected before, on the dynamic analysis of composite blades.

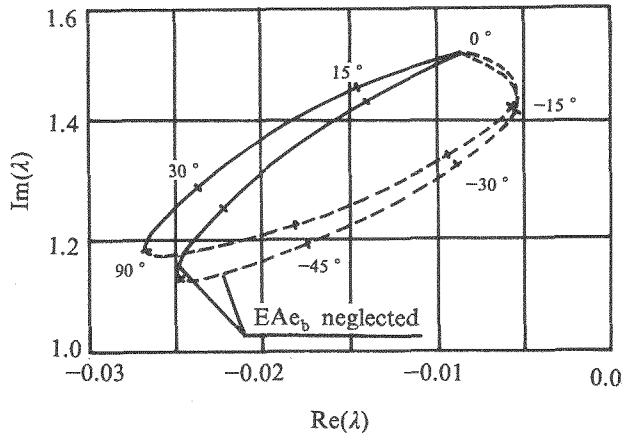

Fig.9 Root locus plots for composite hingeless blade with unsymmetric laminate

Figure 10 presents the root locus plots with changing the ply angle for the symmetric and antisymmetric configurations. In the symmetric model, the laminae for the top one–third thickness and the bottom one–third thickness are all laid up at the same ply angles, whereas the laminae in the remaining inner one–third thickness are oriented at zero ply angles. For the antisymmetric configuration, the laminae in the

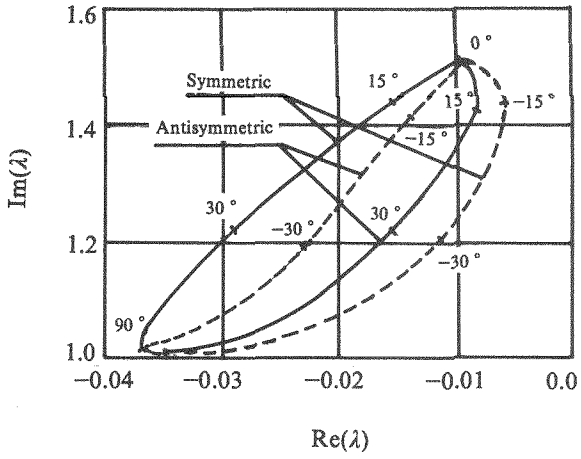

Fig.10 Root locus plots for composite hingeless blade with symmetric and antisymmetric laminates

outer one–third thickness on both sides are laid up at antisymmetric ply angles, such as: if the positive ply angles for the top laminae, the negative ply angles for the bottom ones. The laminae for the remaining inner one–third thickness are also oriented at zero ply angles. From Fig.10, it is seen that

(1) For symmetric configuration the system with the positive ply angles is more stable than that with the negative ones, while for antisymmetric configuration the results is just reversed.

(2) The influence of ply angles for symmetric configuration is more significant on aeroelastic stability than that for antisymmetric one.

Composite Bearingless Rotor Blade

The typical structural model of a composite bearingless rotor blade is shown in Figure 3(b). The fundamental lead–lag, flap, and torsion frequencies for the bearingless configuration with zero ply angles are 1.43, 1.17, and 4.01 respectively. The stability results are calculated for configurations categorized into three cases:

In Case I, beam 1 of the composite flexure is the unsymmetric configuration mentioned above, whereas the laminae of beam 2 are laid–up at zero ply angles.

In Case II, laminated beam 2 in the flexure is the unsymmetric configuration, whereas the laminae of beam 1 are oriented at zero ply angles.

In Case III, both beam 1 and beam 2 of the flexure are the unsymmetric configuration.

The fiber orientations in the outboard blade are kept at zero ply angles in all the cases above.

Figures 11 and 12 correspond to Case I and II respectively. Obviously, either the positive ply angles of beam 1 in Case I or the negative ply angles of beam 2 in Case II stabilize the composite multiple–load–paths system. In general, the variation of ply angles in the flexbeams changes coupling stiffness parameters first, and then influences the dynamic stability of the composite bearingless rotor blade.

For Case III, Figure 13 shows three root locus plots for a composite bearingless blade. The solid and dotted lines represent positive ply angles and negative ply angles respectively .The system is in the most stability only when the ply angle in both flexbeams is equal to 30 degrees. The dash and dot line, in Fig.13, presents the stability of the configuration, where beam 1 and beam 2 have opposite ply angles, i.e. if the laminae in beam 1 are oriented at positive ply angles, the laminae in beam 2 are at negative ply angles. In the mark "±" the top "+" refers to the positive ply angle in beam 1, and the bottom "−" to the negative one in beam 2. Figure 13 indicates that the flexure configuration with positive ply angles in both beam 1 and beam 2 stabilizes the composite bearingless blade more

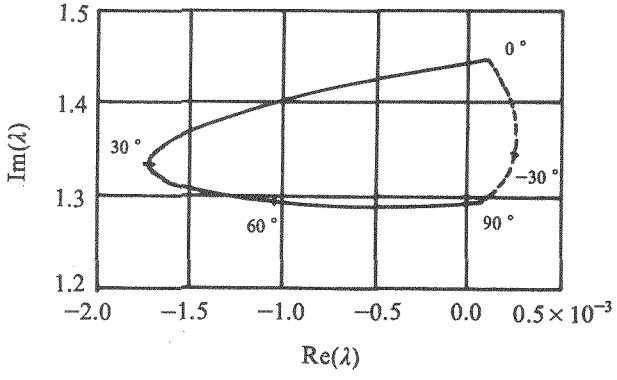

Fig.11 Root locus plot for composite bearingless blade varying with ply angles in beam 1

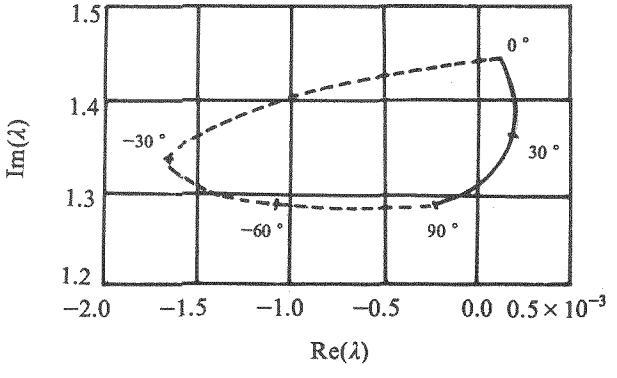

Fig.12 Root locus plot for composite bearingless blade varying with ply angles in beam 2

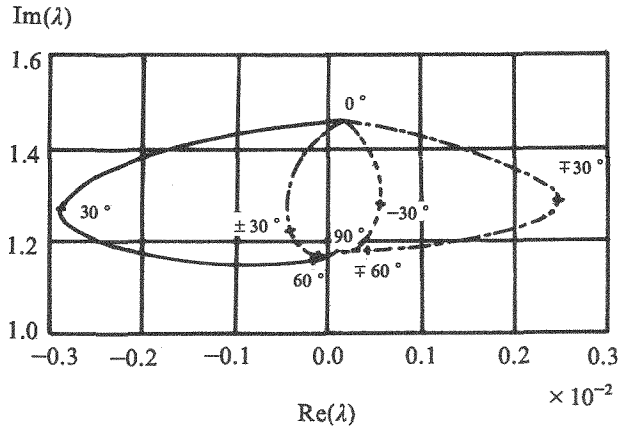

Fig.13 Root locus plots for composite bearingless blade varying with ply angles in both beam 1 and beam 2

significantly than that with positive ply angles in beam 1 and negative ply angles in beam 2, though either the positive ply angle 30 ° in beam 1 (beam 2 at zero ply angle) or the negative ply angle −30 ° in beam 2 (beam 1 at zero ply angle) leads the blade's stability up to the maximum (see Figures 11 and 12). The characteristics described above of the laminated flexure are very useful in desingning and modifying new kinds of composite bearingless rotors.

Conclusion

The aeroelastic stabilities of isotropic bearingless blade, a composite hingeless blade, and a composite bearingless blade in hover are investigated using a finite element formulation. Several important conclusions are obtained as follows

1. The geometrical parameters of the flexure strongly influence the dynamic stability of isotroic bearingless rotor blades.

2. For a composite hingeless blade, the positive ply angles in unsymmetric and symmetric configurations make the system more stable than the negative ones, while the antisymmetric configuration possesses the completely revered behavior.

3. The coupling stiffness constant EAe_b has some influence on the stability of composite rotor blade with unsymmetric configurations.

4. A composite bearingless blade becomes more stable when the ply angles of beam 1 in the flexure are positive (beam 2 at zero ply angle) or the ply angles of beam 2 are negative (beam 1 at zero ply angle)

5. The flexure with positive ply angles in both beam 1 and beam 2 stabilizes the composite bearingless blade more significantly than that with positive ply angles in beam 1 and negative ones in beam 2.

Copyright © 1990 by ICAS and AIAA. All rights reserved.

Finally, it may be deduced that the range of aeroelastic tailoring for the composite bearingless rotor blade is wider than that for the composite hingless rotor blade.

References

(1) Bousman, W.G., Ormiston, R.A., and Mirich, P.H., "Design considerations for Bearingless Rotor Hubs," Presented at the 39th Annual Forum of the AHS, St. Louis, U.S.A, May 1981.

(2) Sivaneri, N.T. and Chopra, I., "Finite Element Analysis for Bearingless Rotor Blade Aeroelasticity," J.AHS, vol.29, No.2,1982.

(3) Mansfield, E.H. and Sobey, A.J., "The Fibre Composite Helicopter Blade, Part 1: Stiffness Properties, Part 2: Prospects for Aeroelastic Tailoring," Aeronautical Quarterly, May 1979, pp.413–449.

(4) Hong, C.H. and Chopra, I., "Aeroelastic Stability Analysis of a Composite Rotor Blade," Journal of AHS, vol.30 No.2 1985, pp.57–67.

(5) Hong, C.H. and Chopra, I., "Aeroelastic Stability of a composite Bearingless Rotor Blade,"J.Am.Helicopter Soc., vol. 4,pp .29–35(1986).

(6) Xu Ming, Xu Guiqi, "Finite Element Analysis of a Laminated Beam With Coupled Bending–Torsional Deflection," Journal of NAI, vol. 19, No.3, 1987, pp. 30–39.

(7) Hodges, D.H. and Dowell, E.H., "Nonlinear Equations of Motion for Elastic Bending and Torsion of Twisted Nonuniform Blades, "NASA TN D–7818, Dec.1974.

(8) Hodges, D.H. and Ormiston, R.A., "Stability of Elastic Bending and torsion of Uniform Cantilever Rotor Blades in Hover with Variable Structural Coupling," NASA TN D–8192, April 1976.